Contribution of Aromatic−Aromatic Interactions to the Anomalous pK_a of Tyrosine-9 and the C-Terminal Dynamics of Glutathione *S*-Transferase A1-1[†]

Catherine Ibarra, Brenda S. Nieslanik, and William M. Atkins*

Department of Medicinal Chemistry, Box 357610, University of Washington, Seattle, Washington 98195-7610

Received April 3, 2001; Revised Manuscript Received June 26, 2001

ABSTRACT: Most cytosolic glutathione *S*-transferases (GSTs) exploit a hydrogen bond between an active site Tyr and the bound glutathione (GSH) cofactor to lower the pK_a of the GSH and generate the nucleophilic thiolate anion, GS⁻. In human (hGSTA1-1) and rat (rGSTA1-1) homologues, the active site Tyr-9 has a low pK_a of 8.1−8.3, for which the functional significance is unknown. Crystal structures of GSTA1-1 suggest that weakly polar interactions between the electropositive ring edge of Phe-10 and the π-cloud of Tyr-9, in the apoenzyme, could stabilize the tyrosinate anion and also modulate the pK_a of GSH. Upon binding a product GSH conjugate, Phe-10 moves away from Tyr-9, allowing the highly dynamic C-terminus to "close" over the active site. To explore the role of Phe-10 in modulating the Tyr-9 pK_a and in ligand binding, rGSTA1-1 mutants F10Y, F10L, and F10A were characterized. The pK_as of Tyr-9 in the apoenzymes were 8.2 ± 0.2, 8.7 ± 0.2, and 9.3 ± 0.1, respectively, for F10Y, F10L, and F10A, compared to 8.3 ± 0.2 for the "wild type". The experimentally determined pK_as qualitatively paralleled the energies required to remove a proton predicted by ab initio calculations using model compounds constrained to the coordinates of rGSTA1-1. The pK_a of GSH in the binary complex was significantly less affected by these substitutions. In contrast, F220I and F220Y C-terminal mutations caused the pK_a of Tyr-9 to decrease modestly. For the binary complex with *S*-hexyl-GSH, which induces the "closed" conformation, Tyr-9 retains a low pK_a and the Phe-10 substitutions have significant effects. Presumably, Phe-10 plays a critical structural role in stabilizing the closed conformation. The mutations F10L and F10A also slowed the rate of GSH conjugate binding by 10−20-fold, as measured by stopped-flow fluorescence. The effects of Phe-10 substitution were large for both steps of the biphasic binding reaction, suggesting the importance of aromatic interactions throughout the reaction coordinate. A unified view of the C-terminal dynamics of GSTA1-1 is discussed, which emphasizes the coupling between Tyr-9 ionization, active site solvation, and C-terminal dynamics.

The cytosolic glutathione *S*-transferases (GSTs) (GSTs)[1] catalyze the conjugation of the tripeptide glutathione (GSH) with a broad range of electrophilic toxins, drugs, and endogenous compounds (*1*, *2*). Several classes of cytosolic GSTs have been identified and characterized (*1*, *2*). In mammals, the various GSTs are designated as A-, M-, P-, T-, K-, and Z-class isoforms. In addition to their differences in structure and function, isoforms from different classes exhibit differential tissue-dependent expression and over-expression in tumors (*3*). A catalytic device common to all cytosolic mammalian GSTs is a hydrogen bond between the thiolate of enzyme-bound GS⁻ and a Tyr or Ser hydroxyl group. This hydrogen bond stabilizes the GS⁻ and effectively lowers the pK_a of the bound GSH from ∼9.3 in bulk aqueous solution to 6.5−7.4 at the active site of various GSTs (*4*, *5*). In principle, differences in the GSH·GST pK_a may contribute to isoform-dependent substrate selectivity as predicted by Bronsted relationships (*6*). However, active site-imposed steric constraints are likely to be the major determinant of substrate selectivity (*7*−*9*).

A unique feature of A-class GSTs is the unusually low pK_a of the catalytic Tyr (*10*−*12*). The spectroscopically determined pK_as are 8.1−8.3 for the human and rat A1-1 isoforms, compared to a pK_a of 10.3 for Tyr in solution. The pK_a for the human A4−4 isoform is even lower, at ∼6.7 (*8*). For the A1-1 isoforms, a highly conserved Arg contributes to the low Tyr pK_a through electrostatic effects (*12*). Upon discovery of the unusual pK_a in the A1-1 isoform, it was suggested that the catalytic Tyr might act as a general base and deprotonate GSH prior to attack of GS⁻ at electrophilic substrates (*10*). However, on the basis of elegant solvent deuterium kinetic isotope studies, the GST M1-1 isoform, for which the catalytic Tyr has a "normal" pK_a, does not include general base catalysis (*13*). Similarly, the kinetic behavior of hGSTA1-1 site-specifically substituted with fluorotyrosine-9 analogues suggests that this isoform does not utilize a general base mechanism (*14*). Rather, the shared

* Corresponding author. Phone: (206) 658-0379. Fax: (206) 685-3252. E-mail: winky@u.washington.edu

[1] Abbreviations: GST, glutathione *S*-transferases (GSTs) exploit a hydrogen ransferase; GSH, glutathione; GS⁻, thiolate anion of GSH; GSO₃⁻, glutathione sulfonate; DEAE, diethylaminoethyl anion exchange; SDS−PAGE, sodium dodecyl sulfate−polyacrylamide gel electrophoresis; CDNB, 1-chloro-2,4-dinitrobenzene; MES, 2-(*N*-morpholino)ethanesulfonic acid; CAPSO, 3-(cyclohexylamino)-2-hydroxy-1-propanesulfonic acid; HEPES, *N*-(2-hydroxyethyl)piperazine-*N*′-2-ethanesulfonic acid; GS−EA, Michael adduct of ethacrynic acid and glutathione; LC-ESI-MS, liquid chromatography−electrospray ionization mass spectrometry; rGST, GST derived from rats; hGST, GST derived from humans.
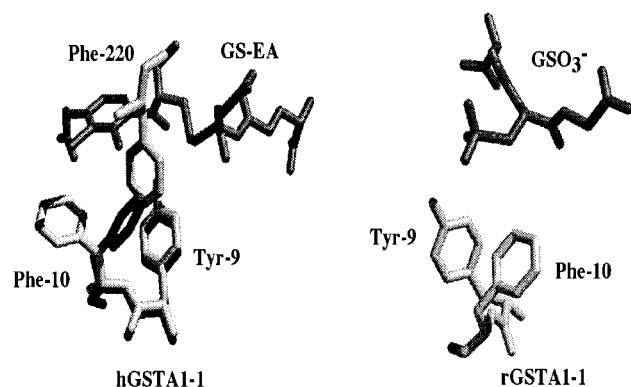
FIGURE 1: Local dynamics of GSTA1-1 near the catalytic Tyr-9. Left: In the apo hGSTA1-1, Phe-10 (black) is above Tyr-9 (black), and the C-terminus is disordered (not visible). Upon addition of the ethacrynic acid conjugate GS−EA, Phe-10 moves to allow Phe-220 within the C-terminal helix to occupy the space above Tyr-9 (structures taken from refs *16* and *17*). Right: The Phe-10/Tyr-9 interaction in the rGSTA1-1·GSO₃⁻ complex (*18*) is similar to that of the human isoform, except the Phe-10 makes a steeper angle with, and is closer to, the center of the aromatic ring of Tyr-9.

proton resides on the phenolic hydroxyl group of the catalytic Tyr-9 throughout the reaction, and the pK_a of Tyr-9 in the wild type is not sufficiently low to impose a mechanistic difference between A-class GSTs and others. Thus, a functional role for the anomalous ionization properties of the catalytic Tyr of A-class GSTs has not been identified.

A dynamic feature that is unique to GSTA1-1 is the ligand-dependent conformational change at the C-terminal segment, which provides a kinetic barrier to binding and dissociation of substrates and products (*15*). X-ray crystal structures (*16, 17*) of the human GSTA1-1 in the presence of GSH product conjugates indicate that the C-terminal 14 residues form a helix which packs the pendant side chain of Phe-220 near Tyr-9 and Phe-10. In contrast, the C-terminal 14 residues are crystallographically invisible in the apoenzyme (*16*) and in the rGSTA1-1·GSO₃⁻ complex (*18*). Furthermore, NMR studies suggest that the C-terminus is heterogeneous until both the G-site and the H-site are occupied (*19, 20*). In the structures for which the C-terminus is disordered, the edge of Phe-10 is packed against the face of Tyr-9, and Phe-10 must be displaced in order for the C-terminal helix to "close" over the active site. The aromatic interactions between Phe-10 and Tyr-9 in the apoenzyme are replaced by less intimate Phe-220/Tyr-9 interactions when the C-terminus closes. The local interactions for the GSTA1-1 are summarized in Figure 1. Mutations at Phe-220 result in modest changes in the pK_as of Tyr-9 and GSH and in the dynamics of the C-terminus (*21−23*). Interestingly, these substitutions modulate the ionization state of Tyr-9 or GSH even though residue 220 is highly disordered in the apoenzyme and in the GSO₃⁻ complex. Also, biochemical studies suggest that a disordered C-terminus contributes to the local active site environment in the GSH complex (*19, 20, 24*).

In the "closed" conformation, Phe-10 provides an additional interaction with Phe-220, which presumably contributes to the stability of the closed state. In fact, Phe-10 is the only residue not contained in the C-terminal helix that undergoes significant rearrangement upon GSH-conjugate binding. Possibly, binding of electrophilic substrates at the hydrophobic substrate "H-site" drives the switch in interactions between Phe-10, Tyr-9, and Phe-220, although this

has not been demonstrated. Although the available structures suggest a critical role for Phe-10 in ligand-dependent C-terminal dynamics and possibly in modulating the ionization properties of Tyr-9, no mechanistic studies concerning the role of Phe-10 GSTA1-1 function have been reported. Notably, mutations at Phe-10 have been obtained by directed evolution to obtain GSTA1-1 variants with altered substrate specificity, but studies of the C-terminal dynamics in these variants were not reported (*25*). Here, we examine in detail the role of Phe-10 in modulating the pK_as of Tyr-9 and GSH, and we demonstrate the critical role of this residue in orchestrating the C-terminal dynamics.

MATERIALS AND METHODS

Chemicals. GSH, CDNB, MES, HEPES, CAPSO, and GSO₃⁻ were obtained from Sigma (St. Louis, MO). GS−EA was synthesized and its purity analyzed as described (*15*).

Site-Directed Mutagenesis. The Phe-10 mutants were constructed by PCR-based amplification of a fragment spanning the *Eco*RI and *Bgl*II restriction sites contained in the linearized pKKGTB34 or pKKGTB34-W21F plasmid. Construction of the pKKGTB34 plasmid has been described previously (*26*). Similarly, the Phe-220 mutants and the C-terminal truncation mutant were constructed by PCR-based amplification of a fragment spanning the *Bgl*II and *Sal*I restriction sites contained in the aforementioned plasmids. The sequences of the oligonucleotide primers encoding the F10Y, F10A, and F10L mutants were 5′-GTGCTTCAC-TAC**TAC**AATG*CTCGAG*GCAGAATGGAG-3′, 5′-GTGCT-TCACTAC**GCC**AATG*CTCGAG*GCAGAATGGAG-3′, and 5′-GTGCTTCACTAC**CTG**AATGCCCGGGGCCAGA-3′, respectively. Indicated in bold letters and italic letters are the mismatched codons and unique *Xho*I sites, respectively. All primers spanned the *Eco*RI site. The final PCR product was digested with *Eco*RI and *Bgl*II and subcloned into pKKGTB34 or pKKGTB34-W21F plasmids that were digested with a similar set of restriction enzymes. Conditions for the PCR reactions were 10 mM (NH₄)SO₄, 20 mM Tris (pH 8.3), 3 mM MgSO₄, 200 μM each dNTP, 0.1% Triton X-100, 10 ng of linearized template, and 1 unit of Vent DNA polymerase (New England Biolabs). The cycle profiles were 94 °C for 1 min, 65 °C for 1 min, and 72 °C for 1 min for 25 cycles, followed by 10 min at 72 °C. All mutants were validated by DNA sequencing.

Protein Expression and Purification. The expression and purification of GSTA1-1 mutants have been described previously (*11*). Briefly, *Escherichia coli* AB1899 cells harboring the plasmid were used to express wild-type or mutant protein. Proteins were purified by using a GSH affinity column and an anion-exchange (DEAE) column. Fractions containing GST were pooled and then chromatographed on a gel filtration column (Sephadex G75) to remove GSH. Mutant proteins purified by this method were >97% pure on the basis of SDS−PAGE analysis. Mutants were analyzed by LC-ESI-MS in order to verify that the C-terminus was not proteolyzed during *E. coli* expression. All mutants were full length.

Ab Initio Model Calculations. Model calculations were performed as described previously (*23*). The Tyr-9 and Phe-10 were modeled as *p*-cresol and benzene, respectively, using the coordinates of the non-hydrogen atoms of rat or human

GSTA1-1 as indicated (PDB codes: IEV4 and 1GUH). Geometry optimization was performed with the Hartree–Fock theory and the 3-21G* basis set. The coordinates of Phe-10 in rGSTA1-1 were used as templates for *p*-cresol-10, isobutane-10, and methane-10 to provide mimics of Tyr-10, Leu-10, and Ala-10, respectively. The structures of these models, in complex with *p*-cresol-9, were optimized as indicated above. Single point energy calculations of the proton affinity were performed with the 6-31+G* basis set. The recovered energies are those required to remove a proton from *p*-cresol-9.

Steady-State Kinetics. Enzymatic activity was determined spectrophotometrically with 1 mM CDNB and 1 mM GSH as described previously (*27*). The kinetic parameters for CDNB and GSH were measured at pH 6.5 and 25 °C, using the following conditions: (a) 0.1–3 mM CDNB in the presence of 1 mM GSH and (b) 0.1–4 mM GSH in the presence of 1 mM CDNB. The k_{cat} and K_M values were determined by fitting the collected data to the Michaelis–Menten equation via the Enzfitter program.

Spectroscopic Determination of Tyr-9 pK$_a$. The pK_a of Tyr-9 was determined by both fluorescence and UV absorbance spectroscopy. Because the pK_a values determined by the two methods were identical within experimental error, only those obtained by fluorescence are reported. Fluorescence titrations were performed as described previously (*11*). Briefly, samples contained 1 μM GST in a mixed buffer of 35 mM MES/35 mM Tris/35 mM CAPSO at various pHs and 25 °C. The pK_a values were determined from the fluorescence intensity at 305 nm of excitation spectra, as well as from the spectral center of mass of emission spectra. Fluorescence titrations were also carried out at 5 °C in the absence and presence of 1.5 mM *S*-hexylglutathione. For difference absorbance spectroscopy, samples contained 10 μM GST in the same mixed buffer system. The absorption intensity at 295 nm due to tyrosinate was monitored at 0.5 pH unit intervals between the pH of 5.5 and 9.5. Titration data were fitted to an equation describing single ionization via Enzfitter.

Spectroscopic Determination of GSH pK$_a$. The pK_a of GSH bound to mutant proteins was determined as described (*4*). Briefly, the UV difference spectra of samples containing 10 μM GST in the absence and presence of 400 μM GSH were determined via a Cary 3E spectrophotometer. Samples were prepared in 50 mM MES/50 mM HEPES/50 mM Tris/1 mM EDTA at various pHs. The spectra of the binary GST·GSH complex were measured between 230 and 300 nm. The absorption intensity at 239 nm due to thiolate was monitored at 0.25 pH unit intervals between pH 5.5 and 8.0.

GST Binding and Dissociation Kinetics. Binding and dissociation experiments were performed via a BioLogic SFM/QFM stopped-flow fluorometer as described previously (*15*). The rate constants for the binding reaction were measured by the decrease in protein fluorescence after rapid mixing of an equal volume of 2 μM GST and 20–400 μM GS–EA at 15 °C. Kinetic data were analyzed and fitted to a single (eq 1) or double (eq 2) exponential decay equation:

$$f(x) = a_1 e^{-k_{obs1}t} + C \qquad (1)$$

$$f(x) = a_1 e^{-k_{obs1}t} + a_2 e^{-k_{obs2}t} + C \qquad (2)$$

where a_1 and a_2 are the amplitudes of two observed rate constants k_{obs1} and k_{obs2}, t is the time, and C is the offset.

Under conditions when two rate constants were experimentally observed, the rapid association and dissociation rates, k_1 and $k_{-1(calc)}$, were fitted to an equation (eq 3) describing linear dependence of k_{obs1} on GS–EA concentration:

$$k_{obs1} = k_{-1(calc)} + k_1[\text{GS–EA}] \qquad (3)$$

The association and dissociation rates of the slower step of the binding reaction, k_2 and $k_{-2(calc)}$, were fitted to an equation (eq 4) describing hyperbolic dependence of k_{obs2} on GS–EA concentration:

$$k_{obs2} = k_{-2(calc)} + \frac{k_2}{1 + (K_1/[\text{GS–EA}])} \qquad (4)$$

In cases where a single rate constant was observed, plots of k_{obs} versus GS–EA concentration also fit best to a hyperbolic curve (eq 5):

$$k_{obs2} = k_{-2(calc)} + \frac{k_2[\text{GS–EA}]}{K_1 + [\text{GS–EA}]} \qquad (5)$$

The dissociation of product from the GST·GS–EA complex was monitored by the increase in fluorescence intensity after rapid mixing of an equal volume of 2 μM complex and 5 mM of the trapping agent, GS-sulfonate (GSO$_3^-$). The dissociation rate constants, $k_{-1(exp)}$ and $k_{-2(exp)}$, were measured directly from a single (eq 1) or double (eq 2) exponential fit to the raw data.

RESULTS

Molecular Basis for the Low pK$_a$ of Tyr-9 in Apo GSTA1-1. It has been shown previously that Arg-15 contributes electrostatic stabilization of tyrosinate-9 of hGSTA1-1 (*12*). However, the pK_a of Tyr-9 for an R15L mutant was ~8.8, significantly below the pK_a of Tyr in solution (10.3). Therefore, we hypothesized that other interactions also contribute to the ionization properties of Tyr-9. An obvious possibility is the first sphere interaction with Phe-10. On the basis of available crystal structures (*16–18*), we hypothesized that the unusually low pK_a of Tyr-9 in GSTA1-1 was due, in part, to stabilization of the tyrosinate-9 by the electropositive ring edge of Phe-10, wherein Phe-10 donates δH$^+$ to the π-cloud of Tyr-9 (Figure 1). It is well established that edge-to-face packing between aromatic rings in proteins is energetically favorable, with interaction energies estimated to be ~0.5–1.0 kcal/mol in solution (*28, 29*). These interactions are analogous to on-face hydrogen bonds and π-cation interactions, although the free energy of interaction is decreased (*30–32*).

The magnitude of aromatic–aromatic interactions is highly dependent on distance and orientation (*28–32*). To determine whether the distance between Phe-10 and Tyr-9 and their relative ring orientation would allow for electrostatic edge-to-face interactions, we performed ab initio calculations with model compounds superimposed on the three-dimensional coordinates of these residues in the apo structure of hGSTA1-1 and the GSO$_3^-$ complex with rGSTA1-1. Tyr-9 was mimicked by *p*-cresol, and benzene was used as a mimic of

Table 1: Gas-Phase Proton Affinities for Tyr-9 from Model Calculations[a]

| | Tyr-9-OH $\rightarrow$ Tyr-9-O$^-$ + H$^+$ | |
model	proton affinity (kcal/mol)	ΔE (kcal/mol)
p-cresol-9	447.05	
human GSTA1-1		
p-cresol-9/benzene-10	365.74	−81.31
rat GSTA1-1		
p-cresol-9/benzene-10	368.44	−78.61
p-cresol-9/*p*-cresol-10	392.47	−54.58
p-cresol-9/cyclohexane-10	394.57	−49.76
p-cresol-9/isobutane-10	471.88	+24.83
p-cresol-9/methane-10	548.82	+101.76

[a] Energy required to remove a proton from Tyr-9. The non-hydrogen atoms of *p*-cresol-9 and benzene-10, which respectively provide mimics of Tyr-9 and Phe-10, were constrained to the coordinates of rGSTA1-1 with bound glutathione sulfonate (*18*). The optimized structures of *p*-cresol-10, isobutane-10, methane-10, and cyclohexane-10 provide mimics of Tyr-10, Leu-10, Ala-10, and nonaromatic residue, respectively. In addition, the non-hydrogen atoms of *p*-cresol-9 and benzene-10 in the hGSTA1-1 model were constrained to the coordinates of the human isoform with bound *S*-benzylglutathione (*17*).

Phe-10. After constraining the heavy atoms to the coordinates of the protein, hydrogens were added and the geometry was optimized. The recovered energies are those required to remove a proton from *p*-cresol-9. With these structures, the proton affinity of the Tyr-9 hydroxyl was calculated. In addition, the mutations of the rat isoforms, F10Y, F10A, and F10L, were mimicked with *p*-cresol, methane, and isobutane, respectively, and the proton affinities of Tyr-9 for each were calculated. Also, cyclohexane was use as a nonaromatic mimic of Phe-10 with approximately the same volume. Interestingly, we observed that the cyclohexane adopted several isoenergetic conformations during geometry optimization. Each of these conformations stabilized the phenolate (tyrosinate-9) more than the methane (Ala-10) or isobutane (Leu-10) but less than the benzene (Phe-10). The results are summarized in Table 1, with an average value reported for several conformations of cyclohexane. It would be expected that the difference in proton affinities for the various analogues, recovered with a gas-phase calculation, would overestimate the absolute magnitude of aromatic−aromatic interactions in the protein active site. In fact, these calculations are not intended to predict pK_a values for the active site Tyr-9 of GSTA1-1 or site-directed mutants discussed below. However, these calculations should provide a reliable qualitative estimate of the sign and relative magnitudes of the energetic effects on the pK_a of Tyr-9 to be expected upon mutation of Phe-10, if significant structural changes did not occur. With increasing ΔE for removal of a proton (less negative to more positive), an increase in Tyr-9 pK_a would be anticipated.

The results indicate that an aromatic ring juxtaposed with Tyr-9, at the distance and orientation observed in the X-ray structures of the rGSTA1-1·GSO$_3^-$, would be expected to lower the pK_a of Tyr-9. Moreover, the model calculations suggest that with aliphatic neighbors, such as alanine (modeled by methane) or leucine (modeled by isobutane), the pK_a of Tyr would be less acidic. The results indicate that edge-to-face aromatic interactions with the orientation of Phe-10 and Tyr-9 observed in the rGSTA1-1 could contribute to the relative stability of the tyrosinate anion.

Table 2: Steady-State Parameters of rGSTA1-1 and Site-Directed Mutants

enzyme	k_{cat} (s^{-1})	K_M (μM)	k_{cat}/K_M (mM^{-1} s^{-1})
	CDNB		
WT[a]	52 ± 2	560 ± 60	93 ± 6
W21F[a]	47 ± 5	520 ± 50	90 ± 9
F10Y:W21F	43 ± 2	753 ± 119	57 ± 2
F10A:W21F	12 ± 1	585 ± 119	20 ± 4
F10L:W21F	25 ± 2	479 ± 66	51 ± 1
W21F:F220Y	55 ± 7	410 ± 40	134 ± 14
W21F:F220I	14 ± 2	300 ± 14	47 ± 6
	GSH		
WT[a]	51 ± 2	310 ± 30	164 ± 12
W21F[a]	62 ± 6	370 ± 30	167 ± 12
F10Y:W21F	43 ± 1	1014 ± 133	42 ± 1
F10A:W21F	12 ± 1	714 ± 94	17 ± 3
F10L:W21F	26 ± 1	551 ± 98	47 ± 3
W21F:F220Y	65 ± 7	331 ± 19	196 ± 19
W21F:F220I	14 ± 2	330 ± 31	42 ± 7

[a] Values taken from ref *44*.

Similar calculations with the coordinates of the human GSTA1-1 emphasize the importance of the orientation of aromatic rings in edge-to-face interactions. In the human enzyme, Phe-10 is oriented toward Tyr-9 at a less steep angle compared to the Phe-10 of the rat isoform. For the human enzyme, Phe-10 is more parallel with Tyr-9, and it is translated toward the phenolic hydroxyl group. With this position, the model calculations suggest that the pK_a of Tyr-9 would decrease, compared to the rat enzyme, albeit by a very small amount (Table 1). Interestingly, this is observed experimentally (*12*, vide infra). It is possible that a direct electrostatic interaction between the edge of Phe-10 and the hydroxyl group of Tyr-9 contributes to the low pK_a in the human isoform, with a decreased contribution from any effect transmitted through the aromatic ring of Tyr-9. However, these gas-phase calculations cannot be used to dissect small differences in the rat and human isoforms. Also, it was observed that if the coordinates of Phe-10 of the hGSTA1-1 were not constrained to the crystal structure of the protein, then the Phe-10 ring moved closer to the Tyr-9 ring and turned to make a steeper angle, thus optimizing the edge-to-face interactions by placing a proton directly over the center of Tyr-9. This observation underscores the contribution of such interactions in some conformations.

Characterization of F10Y, F10L, and F10A Mutants. To probe the hypothesized role of edge-to-face interactions between Phe-10 and Tyr-9 in rGSTA1-1, three amino acid substitutions were made, F10Y, F10L, and F10A. Here we have utilized the previously described W21F mutant as a "wild-type" template. Kinetic parameters for true wild type and the W21F are compared in Table 2. The W21F provides a protein with no tryptophans, thus facilitating spectroscopic characterization of Tyr-9. Unless otherwise noted, the W21F protein is the wild-type reference for the spectroscopic studies (in contrast, for the stopped-flow studies below, where the true wild type is used as a reference).

The F10Y mutant would be expected to retain the edge-to-face interactions observed in the W21F, whereas the F10A and F10L mutants would reduce the electrostatic interactions provided by Phe-10 with the face of Tyr-9. As part of the initial characterization of these mutants, steady-state kinetic parameters were determined for the reaction in which

1-chloro-2,4-dinitrobenzene (CDNB) is conjugated to GSH. The recovered parameters are summarized in Table 2. As always, it is difficult to interpret steady-state kinetic parameters in terms of individual steps of the reaction cycle. However, it is clear that mutations result in a modest change in K_M for CDNB and a more pronounced increase in K_M for GSH. A more obvious change accompanying mutation is the pronounced decrease in k_{cat} for the F10A substitution. As discussed below, the effects on k_{cat} are due, presumably, to an increase in the pK_a of GSH at the active site and also to alterations in ligand-dependent desolvation. The effects on K_M are likely to result from alterations in the substrate-dependent conformational changes in the C-terminus and at Phe-10. For comparison, two mutations at Phe-220 were also studied. For the aliphatic F220I, a significant decrease in k_{cat} was observed.

Spectroscopic Determination of Tyr-9 pK_a. The pK_a of Tyr-9 was determined for each mutant and compared to wild type by the fluorescence methods we have previously described (*10, 11*). Briefly, this method exploits different absorption and emission properties of tyrosine vs tyrosinate. Tyrosine has absorption maxima at 225 nm ($\epsilon = 8200$ cm^{-1} M^{-1}) and 278 nm ($\epsilon = 1350$ cm^{-1} M^{-1}), compared to the absorption maxima for tyrosinate at 295 nm ($\epsilon = 2350$ cm^{-1} M^{-1}) and 245−255 nm ($\epsilon = 11\,000$ cm^{-1} M^{-1}). The emission maximum for tyrosine ranges from 305 to 315 nm vs 330−350 nm for tyrosinate. By monitoring both excitation and emission wavelengths, contribution from tyrosinate can be assigned unambiguously. Figure 2 summarizes typical excitation spectra for the wild type and mutants at several pHs. These results are summarized in Table 3. The pK_a of Tyr-9 was also determined by UV spectroscopy for each mutant (*12*). The pK_as determined by this method were identical to those obtained by fluorescence titration. As hypothesized, the pK_a of Tyr-9 in the F10Y mutant was not significantly increased. In fact, the mean pK_a value was slightly lower than the W21F Tyr-9 pK_a. In contrast, the F10A mutant exhibited a pronounced increase in Tyr-9 pK_a to 9.3, corresponding to an increase in $\Delta\Delta G$ for ionization of Tyr-9 of +1.4 kcal/mol for the mutant. The pK_a of F10L is also increased, although to a lesser extent than observed with the F10A, with a $\Delta\Delta G$ for ionization of +0.5 kcal/mol.

For comparison, the pK_a of Tyr-9 was determined also for mutants with substitutions at Phe-220. As noted above, X-ray structures indicate that Phe-220 replaces Phe-10 in the helix-closed conformation with GSH conjugates bound. The F220Y and F220I substitutions decreased the pK_a of Tyr-9 in the apo rat GSTA1-1 (Table 3). This is analogous to results reported by Gustafsson et al. for the human isoform with F220A and F220T mutants (*22*). It is striking that substitution with nonaromatic groups at Phe-10 had the opposite effect on Tyr-9 pK_a than substitutions at Phe-220. Together, the results indicate that aromatic interactions between Phe-10 and Tyr-9 are necessary and sufficient to lower the pK_a of the later in GSTA1-1. In contrast, aromatic interactions in the apoenzyme involving Phe-220 are not necessary, and the pK_a of Tyr-9 is even lower with a nonaromatic residue present at position 220 (*21, 22*; Table 3).

Ionization Properties of Tyr-9 in GST·S-Hexyl-GSH. As described, the Phe-10/Tyr-9 interactions in the apoenzyme
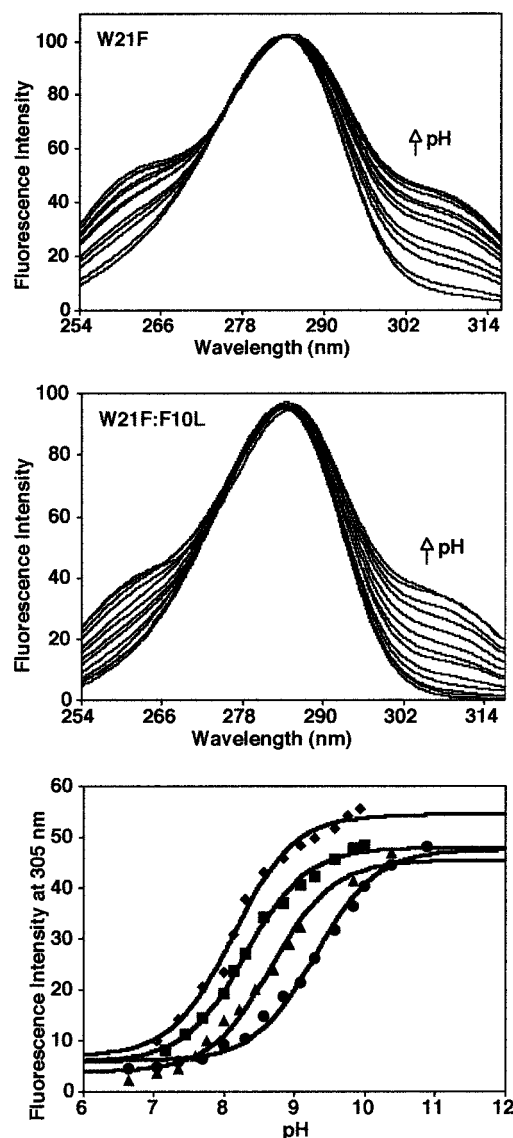

FIGURE 2: Titration of Tyr-9 in Phe-10 mutants. Fluorescence excitation spectra of W21F and W21F:F10L at variable pHs. The excitation bands at 258 and 305 nm result from tyrosinate-9 formation. Titration curves for tyrosinate formation in W21F (squares), W21F:F10Y (diamonds), W21F:F10L (triangles), and W21F:F10A (circles). The recovered pK_a values are reported in Table 3.

Table 3: pK_a Values for Tyr-9 in Disordered and Ordered States

enzyme	pK_a Tyr-9[a] open	$\Delta\Delta G$[b] (kcal/mol)	pK_a Tyr-9[c] closed	$\Delta\Delta G$[d] (kcal/mol)
rW21F	8.3 ± 0.2		8.7 ± 0.1	
rW21F:F10Y	8.2 ± 0.2	−0.1	9.2 ± 0.1	+0.8
rW21F:F10A	9.4 ± 0.1	+1.4	9.6 ± 0.1	+1.3
rW21F:F10L	8.7 ± 0.1	+0.5	9.5 ± 0.1	+1.2
rW21F:F220Y	7.9 ± 0.1	−0.3	8.3 ± 0.1	−0.3
rW21F:F220I	7.7 ± 0.2	−0.6	8.4 ± 0.1	−0.2
rΔ209−222	8.0 ± 0.2	−0.2	ND[e]	ND

[a] pK_a for the apoenzyme. [b] $\Delta\Delta G = (-RT \ln K_a)$ for apo W21F minus $(-RT \ln K_a)$ for the apo form of the mutant entry. [c] pK_a for the Tyr-9 in the presence of 1.5 mM S-hexyl-GSH. [d] $\Delta\Delta G = (-RT \ln K_a)$ for the W21F·S-hexyl-GSH complex minus $(-RT \ln K_a)$ for the S-hexyl complex of the mutant entry. [e] ND = not determined.

are replaced by Phe-220/Tyr-9 in several GSH-conjugate bound structures with the C-terminus closed. In these structures, the Phe-220/Tyr-9 interaction is less intimate than
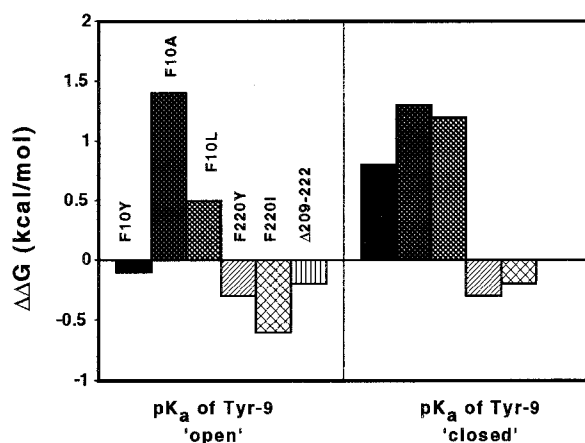
FIGURE 3: Effects of Phe-10 and Phe-220 substitutions on ΔG for ionization of Tyr-9. In the apoenzyme and the *S*-hexyl-GSH complex, the nonaromatic mutations cause an increase in Tyr-9 pK_a. Mutations within, or truncation of, the C-terminus have the opposite effect.

Table 4: pK_a Values of the Thiol Group of Enzyme-Bound Glutathione in rGSTA1-1 and Site-Directed Mutants

enzyme	pK_a of GSH	enzyme	pK_a of GSH
W21F	7.46 ± 0.06	W21F:F220Y	7.02 ± 0.05
F10Y:W21F	7.38 ± 0.08	W21F:F220I	8.32 ± 0.04
F10A:W21F	7.76 ± 0.18	$\Delta209-222$	7.72 ± 0.11
F10L:W21F	7.73 ± 0.13		

the Phe-10/Tyr-9 case. The Phe-220 ring is not within van der Waals radius of Tyr-9. Rather, the ring edge is ~3 Å from the center of the Tyr-9 ring. In this position, Phe-220 could provide weak electrostatic stabilization of Tyr-9 in a fashion directly analogous to Phe-10. In the closed conformation, Phe-10 would not be able to lower the pK_a of Tyr-9 by the edge-to-face interaction observed in the "open" form. However, to the extent that Phe-10 is replaced by Phe-220, the pK_a of Tyr-9 might be expected to remain low. To examine this possibility, we measured the pK_a of Tyr-9 with *S*-hexyl-GSH bound. This ligand induces closure of the C-terminus (*18*; unpublished crystallographic data). The results also are summarized in Table 3 and Figure 3. We have previously suggested that the pK_a of Tyr-9 in the GST· *S*-hexyl-GSH complex is raised significantly to ~9.3, based on fluorescence titration. However, with the absorbance method and more detailed fluorescence analysis, we observe that the Tyr-9 pK_a remains significantly below the pK_a of free Tyr. A striking result is that the pK_a of Tyr-9 increases only 0.5 pK_a unit for the wild type upon addition of a ligand that causes closure of the C-terminus. Thus, with conjugate bound, the pK_a of Tyr-9 remains lower than normal Tyr, and ~5% of the complex remains unprotonated at equilibrium at pH 7.4. Moreover, nonaromatic mutations at Phe-10, F10A, and F10L have qualitatively the same effect on the Tyr-9 in the apoenzyme as for the bound Tyr-9 rGSTA1-1. In contrast, the F10Y mutation results in an increase in the pK_a of Tyr-9 only for the bound state compared to wild type.

As with the apoenzyme, substitution at Phe-220 causes an increase in Tyr-9 pK_a in the *S*-hexyl-GSH complex with a closed C-terminus. However, the pK_a remains lower than the W21F·*S*-hexyl-GSH complex. Thus, the pK_a of Tyr-9 in the closed conformation can be driven lower by removal of the aromatic residue at Phe-220. Apparently, the aromatic−aromatic interactions between Phe-10/Tyr-9 in the apoenzyme are not functionally replaced by Phe-220/Tyr-9 interactions in the closed conformation. However, Phe-10 is required also to maintain a low Tyr-9 pK_a in the closed complex, presumably by anchoring the C-terminus in its closed conformation.

Spectroscopic Determination of the GST·GSH pK_a. In principle, the pK_a of Tyr-9 in the apoenzyme could be a critical determinant of the pK_a of GSH to which it is hydrogen bonded. With decreasing acidity of Tyr-9, the $-OH \cdots {}^- SG$ hydrogen bond would be expected to weaken, with a resulting increase in the pK_a of GSH. Because the available data suggest that the Phe-10/Tyr-9 interactions are maintained in the GSTA1-1·GSH complex, mutations at Phe-10 would be expected to alter the pK_a of GSH. To explore this hypothesis, the pK_a of the GSTA1-1·GSH binary complex was determined by UV difference spectroscopy at 239 nm for each of the F10 mutants as described previously (*4, 22, 23*). These results are summarized in Table 4. The pK_a of GSH for the W21F:F10Y mutant was not significantly altered from the wild-type (W21F) value, as expected for a mutant with no significant change in the Tyr-9 pK_a. Interestingly, the pK_a of GSH was increased for the W21F:F10A and W21F:F10L mutants, but the magnitude of the ΔpK_a (0.3 unit) is small. Although this change is outside the range of experimental error, it is less pronounced than the effect on Tyr-9 pK_a. From the limited data set with W21F and Phe-10 mutants, a linear free energy relationship ($r^2 = 0.88$) is obtained with pK_a of GSTA1-1·GSH vs pK_a of Tyr-9 (apo form). The Bronsted coefficient is $\alpha = 0.37$, reflecting the contribution of the Tyr-9 hydrogen bond to the GSH ionization.

Ionization Properties of a C-Terminal Truncation Mutant. X-ray structures suggest an absence of specific interactions between the C-terminus and active site residues in the apoenzyme and the GSTA1-1·GSO$_3^-$ complex (*16−18*). However, substitution at Phe-220 results in modest changes to the pK_as of Tyr-9 and GSH via a poorly understood mechanism (*21, 22*). By analogy, the observed changes caused by the F10A substitution could, in principle, be due to indirect effects transmitted through the C-terminus. For example, substitution at Phe-10 could alter the conformational space near Tyr-9 that is sampled by the C-terminus and thereby lead to altered pK_as for Tyr-9 or GSH. Therefore, we directly measured the pK_as of Tyr-9 and GSH for a C-terminal truncation mutant which lacks the last 13 residues, $\Delta209-222$. C-Terminal truncation mutants of GSTA1-1 or GSTA2-−2 have been studied by several laboratories and have been found to be structurally intact but functionally impaired (although not completely inactive; see refs *15* and *32*). The binding and dissociation of the product conjugate formed from GSH and ethacrynic acid (GS−EA) with this $\Delta209-222$ mutant have been characterized previously by stopped-flow kinetics (*15*). This mutant retains catalytic activity (~20% of the wild-type specific activity) and binds and releases GS−EA more rapidly than the wild type. The pK_as of Tyr-9 and GSH for this mutant were essentially identical to the wild type and were determined to be 8.07 ± 0.21 and 7.72 ± 0.11, respectively. Apparently, the C-terminus, by itself, does not provide a major determinant of

Scheme 1[a]

$$GST + GS\text{-}R \underset{k_{-1}}{\overset{k_1}{\rightleftharpoons}} [GST{\cdot}GS\text{-}R]_{disordered} \underset{k_{-2}}{\overset{k_2}{\rightleftharpoons}} [GST{\cdot}GS\text{-}R]_{ordered}$$

[a] GS-R = GSH conjugate.

the pK_as of either Tyr-9 or GSH. Thus, the observed effects for the Phe-10 mutants are unlikely to be due to indirect effects transmitted through the C-terminus.

Kinetics of Ligand Binding. The available X-ray structures suggest that Phe-10 would be a critical component of the local, ligand-dependent, dynamics around the active site. Specifically, in order for the C-terminal helix to close completely over the active site, Phe-10 must be displaced from its interaction with Tyr-9 (*16–18*). One interesting possibility would be that the C-terminus adopts a closed conformation, even in the absence of ligand, for the W21F: F10A mutant, inasmuch as the Phe-10 "gate" has been removed. This would shift the conformational ensemble toward "closed but disordered" states and decrease the relative population of open conformations available for ligand docking. Also, the movement of Phe-10 into a hydrophobic pocket formed by Ala-12, Ser-212, and Ala-216 in the closed conformation, in turn, creates a hydrophobic pocket that accommodates Phe-220. Mutations at Phe-10 could destroy the pocket required to stabilize the "closed and ordered" C-terminus. This would lead to a decrease in affinity for ligands and rates of binding. To explore these possibilities, we examined the kinetics of binding of the reporter substrate GS–EA by stopped-flow fluorescence.

As previously described for wild-type rGSTA1-1, hG-STA1-1, and several mutants, binding of GSH conjugates is biphasic (Scheme 1). The first phase corresponds to a bimolecular docking step (k_1, k_{-1}), and the second, slower, phase is a zero-order isomerization reaction that corresponds with closure of the C-terminus in its final ordered state (k_2, k_{-2}) (*15*). For each of the mutants, the concentration dependence of the GS–EA on the observed rate constants was determined, and the individual rate constants k_1, k_{-1}, k_2, and k_{-2} were determined by curve fitting as described in Materials and Methods. For each mutant other than F10Y, the binding and dissociation of GS–EA were clearly biphasic. The conservative mutation F10Y had no deleterious effect on the kinetics. In fact, for the F10Y mutant, the first step was too fast to be observed directly; only the slow steps (k_2, k_{-2}) were observed and were faster than for wild type. In contrast, for F10A and F10L, both steps were significantly slower. The data for the approach to equilibrium after addition of GS–EA to wild type and F10A are shown in Figure 4. Clearly, nonaromatic substitutions at Phe-10 dramatically slow both steps of the ligand binding reaction and decrease the equilibrium binding affinity.

Several laboratories have focused on Phe-220 as a critical player in the C-terminal dynamics. Therefore, we compared the effects of mutation at Phe-10 with the Phe-220 mutants F220Y and F220I. The effects of substitution at Phe-220 were, in general, less pronounced than the effects of mutation at Phe-10. Qualitatively, the Phe-220 substitutions appear to have a greater effect on the second step of the reaction, although the F220I mutation also affects the first step. Because the C-terminus develops tertiary packing interactions
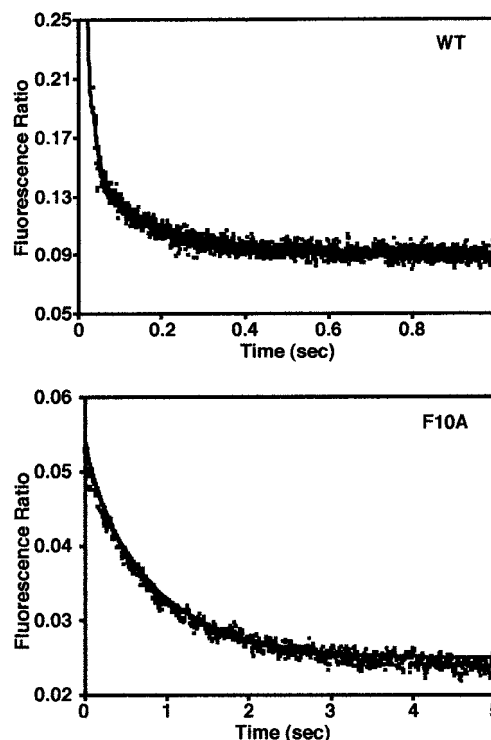

FIGURE 4: Kinetics of binding of GS–EA. The stopped-flow fluorescence data are shown for the approach to equilibrium for wild type (top) and F10A (bottom). Ligand binding and dissociation are slowed dramatically upon substitution at Phe-10. Note the different time scales. The recovered kinetic parameters for all mutants are summarized in Table 4.

Table 5: Kinetic Parameters for GS–EA Binding to rGSTA1-1 WT and Site-Directed Mutants at 15 °C

	WT	F220Y	F220I	F10A	F10Y	F10L
amp$_1$[a]	0.0091	0.0029	0.0074	0.013		0.0045
k_1 (μM^{-1} s^{-1})[b,c]	6.11	7.92	4.81	0.41		0.65
amp$_{-1}$	0.0043	0.0044	0.0037	0.0098		0.0077
$k_{-1(exp)}$ (s^{-1})[d]	15.9	9.37	20.44	8.04		13.3
$k_{-1(calc)}$ (s^{-1})[c]	14.7	6.84	24.22	9.81		14.1
K_1 (μM^{-1})[e]	2.60	1.18	4.25	19.6	2.03	22.1
amp$_2$	0.051	0.082	0.032	0.046	0.034	0.025
k_2 (s^{-1})[c]	17.6	29.6	10.2	0.811	26.3	1.28
amp$_{-2}$	0.018	0.022	0.021	0.013	0.014	0.011
$k_{-2(exp)}$ (s^{-1})[d]	1.51	0.77	4.26	0.59	8.1	0.48
$k_{-2(calc)}$ (s^{-1})[c]	1.89	0.83	6.96	0.51	11.9	0.51
K_2[f]	0.086	0.026	0.42	0.73	0.026	0.42
K_d (μM)[g]	0.19	0.03	1.25	8.25	0.48	6.05

[a] Amplitude values (amp$_1$, amp$_{-1}$, amp$_2$, and amp$_{-2}$) refer to the magnitude of the preexponential terms for the rate constants k_1, $k_{-1(exp)}$, k_2, and $k_{-2(exp)}$, as determined from stopped-flow experiments. [b] The rate constants for all enzymes were determined from duplicate or triplicate experiments, where 15–30 scans were averaged. The standard deviation was less than ±0.8 for k_1, ±0.7 for k_{-1}, ±0.9 for k_2, and ±0.5 for k_{-2}. [c] Kinetic binding and dissociation constants were determined by curve fitting the k_{obs} versus GS–EA plots to eqs 3 and 4. [d] Rates of GS–EA dissociation were determined directly from a fit of the raw data to a single (1) or double (2) exponential equation. [e] K_1 is determined from the ratio $k_{-1(exp)}/k_1$ or eq 5. [f] K_2 is determined from the ratio $k_{-2(exp)}/k_2$. [g] Equilibrium dissociation constants were determined from $K_{d(calc)} = K_1[k_{-2}/(k_2 + k_{-2})]$.

with the remainder of the protein as the reaction progresses to the final closed state, it would be expected that substitutions at Phe-220 would have the largest effects at later stages. The results are summarized in Table 5.

DISCUSSION

The pK$_a$ of Tyr-9 and Bound GSH. The available data suggest that the unusual ionization properties of Tyr-9 are not exploited directly in the catalytic step of the reaction (*13, 14*). However, on the basis of stopped-flow kinetic analysis (*15*) and high-pressure equilibrium experiments (*21*), we have suggested that the unusual pK$_a$ of Tyr-9 *may* play a functional role in controlling the C-terminal dynamics of GSTA1-1, which are critical for ligand binding and rate-limiting product release. In light of the putative functional importance, it is important to establish the molecular basis for the unusual pK$_a$ of Tyr-9. The available X-ray structures and previous mutagenesis studies suggest several local interactions that could contribute in the active site pK$_a$s of GSTA1-1.

One residue of functional importance is Arg-15. Arg-15 is conserved in A-class GSTS, and its guanidino group provides electrostatic stabilization of the GS$^-$ thiolate anion, as well as the tyrosinate-9 anion (*12*). Effects of mutation of Arg-15 of the hGSTA1-1 on the GSH pK$_a$ were not determined spectroscopically, but the Tyr-9 pK$_a$ increased by 0.4, 0.6, and 0.7 pK unit upon substitution with Lys, His, and Leu, respectively. The sulfur of GSH is within 3.8 Å of the guanidinium N$^\epsilon$, and the Tyr-9 hydroxyl in the apo-enzyme is within ~4.8 Å of N$^\epsilon$, so the proposal of an electrostatic effect of Arg-15 on GSH is reasonable.

The results presented here suggest that the C-terminus is not a major determinant of the pK$_a$ of Tyr-9. Substitution at Phe-220 of the rat A1-1 isoform results in only modest changes in the pK$_a$s of both Tyr-9 in the apoenzyme and GSH in its binary complex. Similarly, Gustafsson and co-workers (*22*) observed that mutation at Phe-220 of the human A1-1 resulted in small changes in the pK$_a$ of Tyr-9 and GSH. However, complete removal of the C-terminus, as in the $\Delta 209-222$ mutant, does not cause changes in these pK$_a$ values that are any larger than the point mutations. Thus, the C-terminus contributes to the local environment of Tyr-9 and GSH and "fine-tunes" their pK$_a$s, even when it is disordered or highly dynamic. However, the C-terminus does not provide the major source of stabilization of either tyrosinate-9 in the apoenzyme or GS$^-$ in the binary complex, compared to other structural elements. Although the magnitude of changes in Tyr-9 pK$_a$ accompanying Phe-220 mutations in the rat and human isoforms has been small, each has caused a *decrease* of the Tyr-9 pK$_a$. Thus, if the low pK$_a$ of Tyr-9 serves a function, there is, apparently, no evolutionary driving force to decrease it further.

The current results indicate that Phe-10 is a significant determinant of the unusual pK$_a$ of Tyr-9, albeit not the only determinant. In fact, for the GSTA1-1 isoforms, an aromatic residue at position 10 may be required to maximally lower the Tyr-9 pK$_a$. The ab initio gas-phase calculations demonstrate the potential for weak polar aromatic–aromatic interactions to lower the pK$_a$ of phenol. Electrostatic interactions between the electronegative centroid of aromatic rings and electropositive groups, such as cations or protons, are well appreciated in proteins (*30–32*). Indeed, an example of such an on-face interaction is provided by GSTM1-1, which utilizes a hydroxyl proton from a Thr perched above the ring of Tyr-6 to modulate the pK$_a$ of GSH (*34*). For that isoform, removal of the on-face hydrogen bond by substitu-

tion of the Thr by aliphatic side chains increases in the kinetic pK$_a$ of GSH by 0.7 pK$_a$ unit. This effect was substantially larger than the effect of the F10A or F10L substitutions in the present work, wherein the spectroscopic pK$_a$ of GSH was only increased by 0.3 pK$_a$ unit compared to the template W21F. Apparently, the local environment of different GST isoforms results in differential coupling between the pK$_a$ of Tyr-9 and the pK$_a$ of GSH. It is striking that, for rGSTA1-1, large mutation-induced changes in the pK$_a$ of Tyr-9 are "buffered" so that the change in pK$_a$ of GSH is less pronounced. This appears to contrast the GSTM1-1, where the pK$_a$ of GSH is more sensitive to the electrostatic environment at the face of Tyr-6.

Although the results are consistent with a contribution from an electrostatic edge-to-face interaction that lowers the pK$_a$ of Tyr-9, other forces or explanations must be considered. Possibly, the aromatic ring of Phe-10 is required only to stabilize the local structure near Tyr-9. For example, mutation of Phe-10 may allow Tyr-9 in the apoenzyme to move away from Arg-15 and thus experience an increased pK$_a$. However, this appears unlikely in light of numerous crystal structures that exhibit plasticity with respect to the position of Phe-10, while the position of Tyr-9 remains invariant. The local packing, including the hydrogen bond to the Arg-15 amide, is sufficient to immobilize Tyr-9 even with multiple Phe-10 orientations. Note, however, that, with GSH conjugates bound, Phe-10 may in fact play a "structural" role, wherein it stabilizes the closed conformation (below). Furthermore, we propose that the effect of Phe-10 on the pK$_a$ of Tyr-9 is not due to hydrophobic interactions, per se. Upon substitution of Phe-10 with less bulky Ala and Leu side chains, the hydrophobicity of the Tyr-9 environment is almost certainly decreased, and Tyr-9 is more solvated. If maintenance of a hydrophobic environment were the only role for Phe-10, then substitution with Ala or Leu would cause a decrease in pK$_a$, rather than the observed increase, because ionization of Tyr-9 is more energetically favored in the less hydrophobic, more solvated, environment. Thus, we propose that it is the electrostatic interactions characteristic of aromatic rings that contribute to the low Tyr-9 pK$_a$. Although such edge-to-face interactions are well appreciated for their role in stabilizing protein structure, we are unaware of examples wherein such interactions are used to modulate the pK$_a$ of a catalytic residue.

It should be noted, also, that the local structure at Phe-10/Tyr-9 is not identical for the rGSTA1-1·GSO$_3^-$ complex and apo human GSTA1-1. For the rat complex, Phe-10 is oriented at a steeper angle with Tyr-9, and is further from the phenolic hydroxyl group, than in the human apoenzyme. The angles formed by the rings of Tyr-9 and Phe-10 are ~60° and 40° for the rat and human isoforms, respectively. For the human A1-1, the electropositive ring edge of Phe-10 is significantly closer to the Tyr-9 hydroxyl group and may interact directly rather than via an aromatic on-face effect. Indeed, a direct experimental comparison of rat apo and human apo isoforms yields a modestly lower pK$_a$ value for the human isoform (8.1 vs 8.3, not shown). The ab initio calculations indicate that this may be, in part, due to the difference in orientations of the aromatic rings.

Interestingly, the aromatic–aromatic interactions appear to not be required for a low pK$_a$ of the catalytic Tyr of the GSTA4-4. The catalytic Tyr of GSTA4-4 has been reported

to have a pK_a of ~6.8 (*8*). However, GSTA4-4 has a Pro at the position analogous to Phe-10. Obviously, Pro is not capable of lowering the pK_a of the Tyr via the aromatic edge-to-face interactions. The present work does not provide an explanation for the unusually low pK_a of the "catalytic" Tyr in GSTA4-4. It is interesting that the C-terminus of GSTA4-4 is static and localized to a more open conformation even in the apoenzyme (*35*). Therefore, if the ionization of Tyr-9 is functionally important for controlling the dynamics of GSTA1-1, then this function is not retained in GSTA4-4. In summary, GSTA1-1 and A4-4 isoforms appear to have evolved multiple and different mechanisms for achieving a low Tyr pK_a.

Although direct interactions with Phe-10 are a source of the low pK_a of Tyr-9 in A1-1 when the C-terminus is open, indirect interactions with Phe-10 make a quantitatively greater contribution to the low pK_a of Tyr-9 in the closed conformation (Figure 3). Presumably, this results from Phe-10 anchoring the C-terminus in the closed conformation. In the closed conformation, which is likely desolvated, it is possible that the electrostatic interactions with Arg-15 would be strengthened, thus favoring ionization of Tyr-9 relative to solvated Tyr in bulk solution. In effect, the contribution of Phe-10 to Tyr-9 ionization changes from a direct first sphere electrostatic interaction in the apoenzyme to an indirect second sphere effect in the closed complex. The existence of a low pK_a for Tyr-9 in the closed state has not been considered in detail previously, and the contribution of Phe-10 to the closed conformation has not been examined by mutagenesis.

Dynamics of the C-Terminus. The dynamics of the C-terminus are clearly important for ligand binding and release by GSTA1-1. NMR experiments suggest that Phe-222 in the C-terminus "changes" upon addition of GSH, although the helix is not as ordered as when a GSH conjugate is added (*19, 20*). Furthermore, H-site ligands bind more tightly when the G-site is occupied. Apparently, the G-site is sensitive to the dynamics of the C-terminus. There is a gradient of increased order of the C-terminus upon addition of GSH followed by H-site ligands and occupancy of both the G-site and the H-site. Occupancy of both G- and H-sites is necessary to obtain a completely ordered, closed, C-terminus. Also, the NMR data suggest that the C-terminal helix is not "uniformly" dynamic. The greatest heterogeneity has been suggested to be at Phe-220. These observations are interesting because the available X-ray structures indicate that the C-terminus is a highly dynamic helix in the apoenzyme and in the GSO$_3^-$ binary complex. Apparently, the ensemble of states sampled by the C-terminus allows for local interactions between the residue at Phe-220, GSH, and Tyr-9.

The recovered rate constants k_1, k_{-1}, k_2, and k_{-2} for all of the Phe-10 and Phe-220 mutants (Table 5) can be used to construct relative free energy profiles for the ligand binding reaction with GS—EA (Figure 5). For convenience, the free energies are normalized in the ligand-free complex. Any difference in absolute free energies due to mutation is likely to be negligible in the disordered, uncomplexed, state. It is striking that nonaromatic mutations at Phe-10 significantly slow both the initial docking step (k_1, k_{-1}) and the isomerization of the C-terminus to the closed state (k_2, k_{-2}). The effect on the first step may reflect the role of Phe-10 in

$$GST + GS\text{-}EA \underset{k_{-1}}{\overset{k_1}{\rightleftharpoons}} [GST\;GS\text{-}EA]_{disordered} \underset{k_{-2}}{\overset{k_2}{\rightleftharpoons}} [GST\cdot GS\text{-}EA]_{ordered}$$
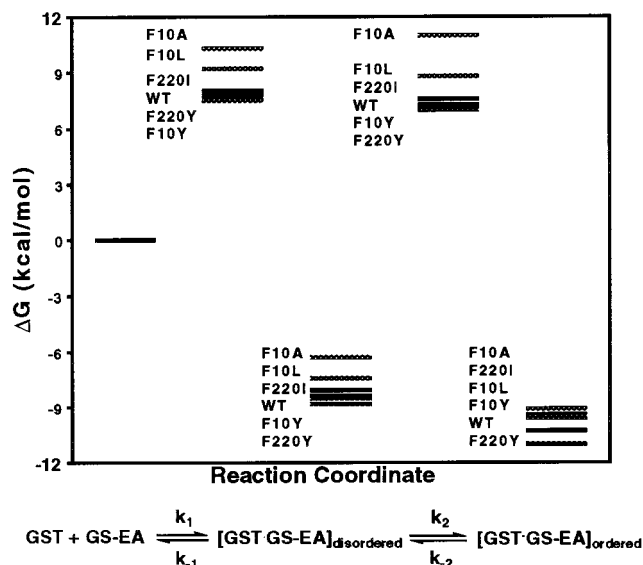
FIGURE 5: Free energy diagram for the reaction coordinate of Phe-10 and Phe-220 mutants. The free energies of the individual proteins have been normalized in the ligand-free state (left).

limiting the conformational space available to the C-terminus in the apoenzyme. On the basis of the available structures, it is likely that Phe-10 in the apo structure sterically blocks the C-terminus from adopting its final closed conformation, as observed in the conjugate-bound structures. With reduction of the steric bulk and elimination of the edge-to-face electrostatic interactions, the F10L and F10A mutants may allow the C-terminus to sample conformations in the apoenzyme that are similar to the closed conformation of the conjugate-bound structures. This would result in an apparent decrease in the rate of the second-order docking step (k_1, k_{-1}), wherein a shift in the preequilibrium toward closed states reduced the concentration of open states available for binding. The effect of Phe-10 substitutions on the second step of the binding reaction (k_2, k_{-2}) is also quite pronounced. The fact that the kinetics of C-terminal closure are affected and not just the equilibrium between open and closed states suggests that Phe-10 plays an important role in guiding the C-terminus to its final closed conformation.

A Unified Model. The results presented here, together with the X-ray structure of the rGSTA1-1 complexed with GSO$_3^-$ (*18*), and suggestions by Gustafsson et al. (*22*) allow for reinterpretation of our previous high-pressure experiments (*21*) and for an initial model summarizing the coupling between the Tyr-9 ionization and C-terminal dynamics. We had speculated, on the basis of pressure-dependent ionization of Tyr-9 together with the observation that Phe-220 could contribute to a low pK_a for GST·GSH, that pressure caused the residue-220 within the disordered C-terminus of GSTA1-1 to interact more strongly with Tyr-9, thus favoring its ionization. This suggestion was also based on the work of Royer et al. (*36, 37*), indicating that "molten globule" states with significant void volume between interstitial spaces in poorly packed structural elements are "high-volume" states compared to folded "native" states. Although some molten globules may have only moderately increased compressibility compared to native states (*38*), others are very sensitive to pressure (*36, 37*). To the extent that the disordered C-terminus of GSTA1-1 has features analogous to molten globules, we suggested the interesting possibility that pressure

would cause the C-terminus to close to a more nativelike, smaller volume, state, with residue-220 juxtaposed to lower the pK_a of GSH through aromatic−aromatic or other electrostatic interactions.

This suggestion was based also on the extreme sensitivity of Tyr-9 to pressure. The observed ionization of Tyr-9 occurred at pressures well below those typically required to unfold proteins or peptides (*39, 40*). At the low pressures found to cause ionization of Tyr-9, proteins do *not* typically unfold, although protein−protein complexes may be disrupted (*39, 40*). In fact, it has been demonstrated that, at such low pressures, proteins "condense" or become more tightly packed, before unfolding at higher pressure (*41*). Our earlier speculation was based also on the observation that substitutions at Phe-220 altered the pK_a of Tyr-9, as confirmed by others (*22*). Inasmuch as Phe-220 was not expected to interact with Tyr-9 when the C-terminus is open, we presumed that interactions between the C-terminus and Tyr-9 would be more prominent with the C-terminus in the closed state.

However, in the apoenzyme, the major determinant of the low Tyr-9 pK_a is Phe-10 rather than Phe-220 (vide infra). The model calculations, supported by the experimental results, provide a significant insight: to the extent that the aromatic Phe-10 lowers the pK_a of Tyr-9 and Phe-10 moves to accommodate C-terminal closure, the C-terminal open conformations must predominate when Tyr-9 is ionized. Thermodynamic linkage requires that ionization of Tyr-9 will strengthen the interaction between Phe-10 and Tyr-9, just as Phe-10 interactions promote ionization of Tyr-9. Therefore, the open conformations with intact Phe-10/Tyr-9 interactions will be favored when Tyr-9 is deprotonated. This is consistent with the observation that the C-terminal truncation mutant has a slightly lower Tyr-9 pK_a than the wild type.

With this new information, our initial speculation concerning the effect of pressure on the C-terminus appears incorrect. More likely, pressure causes the C-terminus to open without necessarily unfolding. Increased solvation of the C-terminus and the active site may be sufficient to provide the observed pressure effects, as with many other systems which undergo denaturation or subunit dissociation at elevated pressure (*39, 40*). This reinterpretation is in accord with the interpretation of Gustafsson et al. (*22*).

Several studies have suggested that the ionization states of Tyr-9 and GSH and the C-terminal conformations are intimately linked (*22, 42*). A model that summarizes the available structural, spectroscopic, and thermodynamic information is summarized in Figure 6. This model is likely to be oversimplified, but it provides a useful template for considering these aspects of GSTA1-1 function. In the apoenzyme and the GSH complex, a dynamic equilibrium may exist with Phe-10 and Phe-220 competing for the space directly adjacent to Tyr-9. At atmospheric pressure in the apoenzyme, the equilibrium favors an open C-terminus with Phe-10 packed against Tyr-9 most of the time. This is suggested also by the X-ray structure of the apoenzyme and the GSO_3^- complex and also by the low pK_a of Tyr-9. When only the G-site is occupied, the dynamics of the C-terminus change, in an as yet undefined way, but the C-terminus does not completely close (*19, 20, 24*). At high pressure, competition between Phe-10 and Phe-220 for the immediate environ-
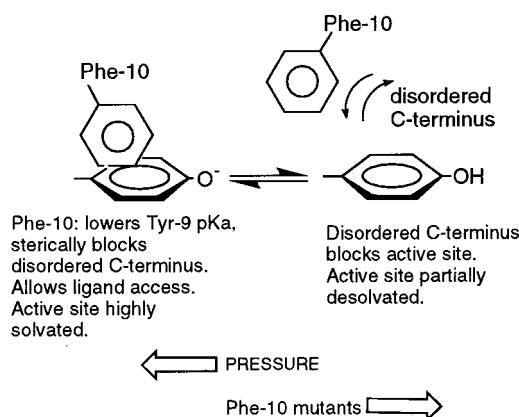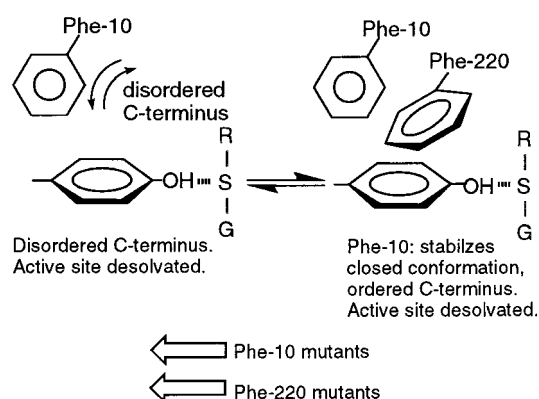

FIGURE 6: Schematic summary of the contribution of Phe-10 to conformational dynamics of the apoenzyme and the complex with a GSH conjugate (R−S−G). Phe-10 directly lowers the pK_a of Tyr-9 in the apoenzyme via edge-to-face interactions. When this interaction is intact, the disordered C-terminus is prevented from sampling conformational space directly over the active site. Phe-10 also stabilizes the closed conformation of the C-terminus in the GSH conjugate complex through interactions with Phe-220. The effects of hydrostatic pressure (from ref *21*) and mutations at Phe-10 and Phe-220 (from refs *21* and *22*) are summarized. The mutant F220Y is an exception. This mutant stabilizes the closed conformation.

ment of Tyr-9 would be decreased as the C-terminus "opened". In turn, the equilibrium conformation of Phe-10 packed against Tyr-9 would predominate to a greater extent than at atmospheric pressure, and the Tyr-9 pK_a would be further reduced. Upon binding a GSH conjugate that drives closure of the C-terminus, Phe-10 remains a critical determinant of C-terminal status and Tyr-9 pK_a. The latter effect is, presumably, due to Phe-10 providing part of a hydrophobic pocket into which Phe-220 is locked. In short, Phe-10 *directly* lowers the pK_a of Tyr-9 and sterically prevents closure of the C-terminus in the apoenzyme and to a lesser extent with the G-site occupied. With both G- and H-sites occupied, however, the new location of Phe-10 provides an *indirect* stabilization the Tyr-9 phenolate, compared to Tyr in solution, and stabilization of the closed conformation.

The modest effects of Phe-220 mutations on Tyr-9 pK_a are likely to be the result of mutation-induced changes in the conformational status of the dynamic C-terminus. Because essentially all mutations at Phe-220 result in a further decrease of Tyr-9 pK_a of the apoenzyme, we presume that

these mutations favor conformations that do not effectively compete with Phe-10 for the space adjacent to Tyr-9 and which provide a more open active site. This is consistent with the increase in on-rate observed for GSH by Gustafsson et al. with F220A and F220T mutants (*22*). However, this is opposite to the effects reported here, where the F220I mutation leads to a decrease in both Tyr-9 pK_a and in rates of GS–EA binding. For both studies, the effect of Phe-220 mutations on ligand binding rates was quite small compared to Phe-10 mutations. The differences in the results probably reflect different conformational requirements for GSH binding vs GSH-conjugate binding. The important point is that these point mutations alter the preequilibrium between states within an ensemble for the apoenzyme, and different conformers preferentially bind ligands, as suggested initially by Gustafsson et al. Interestingly, the F220Y mutation that we described previously (*23*) continues to exhibit "anomalous" behavior. Among the Phe-220 and Phe-10 mutants, it is the only one that has a decreased GSH pK_a and a decreased K_2 value, reflecting a more tightly closed C-terminus. We have suggested the possibility that the F220Y incorporates an on-face hydrogen bond with Tyr-9. It is unlikely that this occurs in the apoenzyme, but such an interaction in the GSH-conjugate-bound structures could be the source of the unusual behavior for this mutant.

Thermodynamic studies suggest that the C-terminus mediates active site desolvation at early stages of the ligand binding reaction coordinate prior to attainment of the closed and ordered conformation (*43*). Presumably, Tyr-9 ionization facilitates solvation of the active site and favors open conformations, whereas Tyr-9 protonation facilitates desolvation and ordering of the C-terminus. Together, the available data indicate that Phe-10 plays a critical role in the coupling between Tyr-9 ionization, active site solvation, and conformational dynamics of the C-terminus.

REFERENCES

1. Hayes, J. D., and Pulford, D. J. (1995) *Crit. Rev. Biochem. Mol. Biol. 30*, 445–600.
2. Armstrong, R. N. (1998) *Curr. Opin. Chem. Biol. 2*, 618–623.
3. Tew, K. D., Monks, A., Barone, L., Rosser, D., Akerman, G., Montali, J. A., Wheatley, J. B., and Schmidt, D. E. (1996) *Mol. Pharmacol. 50*, 149–159.
4. Graminski, G. F., Kubo, Y., and Armstrong, R. N. (1989) *Biochemistry 28*, 3562–3568.
5. Kong, K. H., Takasu, K., Inoue, H., and Takahashi, K. (1992) *Biochem. Biophys. Res. Commun. 184*, 194–199.
6. Nieslanik, B. S., and Atkins, W. M. (1998) *J. Am. Chem. Soc. 120*, 6651–6660.
7. Eaton, D. L., and Bammler, T. K. (1999) *Toxicol. Sci. 49*, 156–164.
8. Nilsson, L. O., Gustafsson, A., and Mannervik, B. (2000) *Proc. Natl. Acad. Sci. U.S.A. 97*, 9408–9412.
9. Dirr, H., Reinemer, R., and Huber, R. (1994) *Eur. J. Biochem. 220*, 645–661.
10. Atkins, W. M., Wang, R. W., Bird, A. W., Newton, D. J., and Lu, A. Y. H. (1993) *J. Biol. Chem. 268*, 19188–19191.
11. Dietze, E. C., Wang, R. W., Lu, A. Y. H., and Atkins, W. M. (1996) *Biochemistry 35*, 6745–6753.
12. Bjornestedt, A., Sternberg, G., Wildersten, M., Board, P. G., Sinning, I., Jones, T. A., and Mannervik, B. (1995) *J. Mol. Biol. 247*, 765–773.
13. Parsons, J. F., and Armstrong, R. N. (1996) *J. Am. Chem. Soc. 118*, 2295–2296.
14. Thorson, J. S., Shin, I., Chapman, E., Stenberg, G., Mannervik, B., and Schults, P. G. (1998) *J. Am. Chem. Soc. 120*, 451–452.
15. Nieslanik, B. S., Dabrowski, M. J., Lyon, R. P., and Atkins, W. M. (1999) *Biochemistry 38*, 6971–698.
16. Cameron, A. D., Sinning, I., L'Hermite, G., Olin, B., Board, P. G., Mannervik, B., and Jones, A. T. (1995) *Structure 3*, 717–727.
17. Sinning, I., Kleywegt, G. J., Cowan, S. W., Reinemer, P., Dirr, H. W., Huber, R., Gilliland, G. L., Armstrong, R. N., Ji, X., Board, P. G., Olin, B., Mannervik, B., and Jones, A. (1993) *J. Mol. Biol. 232*, 192–212.
18. Adman, E. T., Le Trong, I., Stenkamp, R. E., Nieslanik, B. S., Dietze, E. C., Tai, G., Ibarra, C., and Atkins, W. M. (2001) *Proteins: Struct., Funct., Genet. 42*, 192–200.
19. Lian, L.-Y. (1998) *Cell. Mol. Life Sci. 54*, 359–362.
20. Allardyce, C. S., McDonagh, P. D., Prescott, A., Roberts, G. C. K., and Lian, L. Y. (2000) *Clin. Chem., Enzymol. Commun. 8*, 239–253.
21. Atkins, W. M., Dietze, E. C., and Ibarra, C. (1997) *Protein Sci. 6*, 873–881.
22. Gustafsson, A., Etahadieh, M., Jemth, P., and Mannervik, B. (1999) *Biochemistry 38*, 16268–16275.
23. Dietze, E. C., Ibarra, C., Dabrowski, M. J., Bird, A., and Atkins, W. M. (1996) *Biochemistry 35*, 11938–11944.
24. Allardyce, C. S., McDonagh, P. D., Lian, L. Y., Wolf, C. R., and Roberts, G. C. (1999) *Biochem. J. 343*, 525–531.
25. Hansson, L. O., Widersten, M., and Mannervik, B. (1999) *Biochem J. 344*, 93–100.
26. Wang, R. W., Pickett, C. B., and Lu, A. Y. H. (1989) *Arch. Biochem. Biophys. 269*, 536–543.
27. Habig, W. H., Pabst, M. J., and Jakoby, W. B. (1974) *J. Biol. Chem. 249*, 7130–7139.
28. Burley, S. K., and Petsko, G. A. (1988) *Adv. Protein Chem. 39*, 125–141.
29. Burley, S. K., and Petsko, G. A. (1985) *Science 229*, 23–28.
30. Mecozzi, S., West, A. P., Jr., and Dougherty, D. A. (1996) *Proc. Natl. Acad. Sci. U.S.A. 93*, 10566–10571.
31. Mitchell, J. B., Nandi, C. L., McDonald, I. K., Thornton, J. M., and Price, S. L. (1994) *J. Mol. Biol. 239*, 315–331.
32. Gallivan, J. P., and Dougherty, D. A. (1999) *Proc. Natl. Acad. Sci. U.S.A. 96*, 9459–9464.
33. Mannervik, P. G., and Mannervik, B. (1991) *Biochem. J. 327*, 593–600.
34. Liu, S., Ji, X., Gilliland, G. L., Stevens, W. J., and Armstrong, R. N. (1993) *J. Am. Chem. Soc. 115*, 7910–7911.
35. Bruns, C. M., Hubatsch, I., Ridderstrom, M., Mannervik, B., and Tainer, J. A. (1999) *J. Mol. Biol. 288*, 427–439.
36. Vidugiris, G. J., and Royer, C. A. (1998) *Biophys J. 75*, 463–470.
37. Vidugiris, G. J, Markley, J. L., and Royer, C. A (1995) *Biochemistry 34*, 4909–4912.
38. Nolting, B., and Sligar, S. G. (1993) *Biochemistry 32*, 12319–12323.
39. Weber, G. (1986) *Biochemistry 25*, 3626–3631.
40. Atkins, W. M. (1994) *Biochemistry 33*, 14965–14973.
41. Cioni, P., and Strambini, G. B. (1996) *J. Mol. Biol. 263*, 789–799.
42. Nieslanik, B. S., and Atkins, W. M. (2000) *J. Biol. Chem. 275*, 17447–17451.
43. Nieslanik, B. S., Ibarra, C., and Atkins, W. M. (2001) *Biochemistry 40*, 3536–3543.
44. Wang, R. W., Newton, D. J., Pickett, C. B., and Lu, A. Y. H. (1992) *Arch. Biochem. Biophys. 297*, 86–91.